THE ASTROPHYSICAL JOURNAL, 417:209–219, 1993 November 1

IMPROVED OBSERVATIONS OF FAINT PLANETARY NEBULAE IN THE MAGELLANIC CLOUDS

GEORGE H. JACOBY[1]
Kitt Peak National Observatory, National Optical Astronomy Observatories,[2] P.O. Box 26732, Tucson, AZ 85726

AND

JAMES B. KALER
Department of Astronomy, University of Illinois, 103 Astronomy Building, 1002 West Green Street, Urbana, IL 61801
Received 1992 October 19; accepted 1993 May 10

ABSTRACT

The accuracy of spectrophotometry for Magellanic Cloud planetary nebulae is limited by a number of physical effects and operational difficulties: atmospheric dispersion, wavelength-dependent seeing, pointing and guiding errors, and a background of numerous stars and diffuse emission. We describe procedures to minimize the impact of some of these. We then compare our results for both bright and faint objects with published values. There are a few exceptional cases (e.g., LMC 89), but generally we find that bright planetary nebulae in the Clouds have been observed with high accuracy. On the other hand, observations of the faint sample from Jacoby (1980) suffer seriously from many of these effects.

We also compare published λ5007 photometry with new CCD photometry for nine faint planetary nebulae. We find the photographic photometry presented by Jacoby (1980) to be accurate to 0.26 mag. Fluxes for the fainter objects that are derived from spectrophotometry (Boroson & Liebert 1989) are found to be less reliable. In comparison, spectrophotometry using the observational techniques presented in this paper provides reliable absolute fluxes.

With these improved observations, we review the correlations presented by Kaler & Jacoby (1990, 1991) between abundance ratios and central star mass. The new results fit our earlier correlation for N/O, strengthen that for He/H, and change little about those for C/O and O/H.

Subject headings: Magellanic clouds — planetary nebulae: general

1. INTRODUCTION

Planetary nebulae (PNs) that are observed in external galaxies are typically among the very brightest, simply because PNs as a class are not very luminous sources. This is particularly true with regard to abundance studies where spectroscopy of faint lines (e.g., [O III] λ4363) is needed to derive accurate results. The most common PNs, however, such as the majority in the solar neighborhood, intrinsically have the faintest surface brightnesses (Jacoby 1980) because central stars have very short lifetimes during their luminous phase. Consequently, comparisons between the characteristics of nearby Galactic PNs with those in other galaxies have been difficult to interpret (e.g., estimating the fraction of Type I PNs).

High quality data have been presented recently by Meatheringham & Dopita (1991a, b), Monk, Barlow, & Clegg (1988), Aller et al. (1987), and Vassiliadis, Dopita, & Morgan (1992) for PNs in the nearest galaxies, the Magellanic Clouds (MC). These authors have demonstrated that the brighter nebulae can be observed extremely well; agreement across the various observing teams is extremely good for most objects. There are, though, some objects for which the published spectral line ratios are dramatically different, such as object LMC 89 in the catalog of Sanduleak, MacConnell, & Philip (1978). Potential causes of the disagreement are explored in this paper, as they are likely to become more pronounced as the objects under study push to the fainter limits typical of nearby Galactic PNs. [The nomenclature for PNs in the Clouds is hopelessly confusing. Throughout this paper, we will refer to the Sanduleak et al. 1978 catalog of objects by the catalog numbers preceded by either LMC or SMC (i.e., LMC 89). Objects from the Jacoby 1980 catalog will be referred to in a similar fashion but with a "J" prepended to the catalog number (i.e., LMC J35).]

There has been very little work on the faintest PNs in the MC (i.e., the sample of Jacoby 1980) as a consequence of the limited availability of the necessary large telescopes. Observations of PNs that are 6 mag fainter than the brightest objects naturally have been given a lower priority. Neverthless, Boroson & Liebert (1989) presented spectra and Hβ fluxes for all true PN in Jacoby's sample. These data represent an important beginning in the study of the more common class of PNs.

The importance of studying the fainter PNs has been demonstrated by Kaler & Jacoby (1990, 1991) and Dopita & Meatheringham (1991). Both groups find systematic differences in the PN abundances and central star properties between the bright and faint MC samples. For example, the fainter objects generally exhibit more intense enrichment through dredge-up than the brighter objects. The degree of enrichment correlates with central star mass (nitrogen-rich objects invariably have more massive central stars), but higher quality data are needed to demonstrate convincingly that some of the relationships (e.g., variations of O/H with central star mass) suspected by Kaler & Jacoby (1991) are real. An additional attraction of the fainter PNs is that these are more likely to be large and spa-

[1] Visiting Astronomer, Cerro Tololo Inter-American Observatory, National Optical Astronomical Observatories, operated by the Association of Universities for Research in Astronomy, Inc., under contract with the National Science Foundation.

[2] Operated by the Association of Universities for Research in Astronomy, Inc., under cooperative agreement with the National Science Foundation.

tially resolved; this sample at a known distance offers a singular opportunity to tie together kinematic time scales with central star model evolutionary time scales.

In order to study these effects, additional reliable data are needed. Data collection for the bright objects has been relatively easy except for a few instances; however, the faint objects in the MC suffer from special problems that could introduce systematic errors into the derived line ratios and absolute fluxes. We discuss these in § 2 and detail our observational approach to solving them in § 3. We compare our results with values in the literature in § 4.

2. THE OBSERVATIONAL PROBLEMS

Filippenko (1982) demonstrated that aligning the slit angle of a spectrograph with the direction of the atmospheric dispersion dramatically improves the accuracy of spectrophotometry and line ratio measurements. While we adopt this approach in our spectroscopy, there are second-order effects to keep in mind.

First, as Filipenko pointed out, atmospheric dispersion produces an extended image of the object in which the blue light is separated from the red light along the slit and, in turn, on the detector. Consequently, the trace of the spectrum on the detector becomes a function of zenith distance. If this effect is ignored, then a systematic difference will arise, for example, when comparing objects at high air mass with standard stars observed at a lower air mass. While it is straightforward to trace and extract the spectrum of a continuum source, the emission-line spectra of PNs present an added complexity.

The simplest strategy to circumvent this problem, and the one which we adopt, is to extract a much wider than optimal swath (7.5 arcsec in our case) of spectrum from the two-dimensional data. This has the negative impact of reducing the signal-to-noise ratio because more background (sky plus host galaxy light) is included in the extraction swath than would be included by an optimal extraction technique. On the positive side, this technique averages out any spatial variations in the spectrum along the slit. This might arise, for example, in an extended PN having ionization structure. The wide extraction swath also simulated a large aperture that yields a good estimate of the absolute flux.

There are, though, higher signal-to-noise alternatives. The slit can be rotated slightly from the parallactic angle in order to place a random field star (i.e., a continuum source) somewhere on the slit. This serves as a tracer of the atmospheric effects during the spectral extraction procedure (M. Phillips 1992, private communication). A similar approach suggested by Filippenko (1993, private communication) is to take a short exposure of a bright star in the vicinity of the target PN to serve as the tracer. We have not investigated either alternative, however.

Second, atmospheric seeing produces larger images in the blue than in the red, roughly increasing as $(1/\lambda)^{0.2}$ (Fried 1966; Boyd 1978). Thus, more blue light than red light is scattered out of the slit, resulting in a systematic underestimate of the blue flux *unless* the slit is much larger than a seeing diameter. For example, the seeing diameter at λ3727 is 12% larger than at λ6563 (assuming the above functionality). We see from Figure 1 that for a seeing size (i.e., FWHM) of 1 arcsec, and a slit that is 1.5 arcsec wide, the light loss will be 4% greater for [O II] λ3727 relative to Hα assuming that the object is perfectly centered in the slit. A centering error of 0.5 arcsec would increase this deviation to 10%. Our solution to this problem is

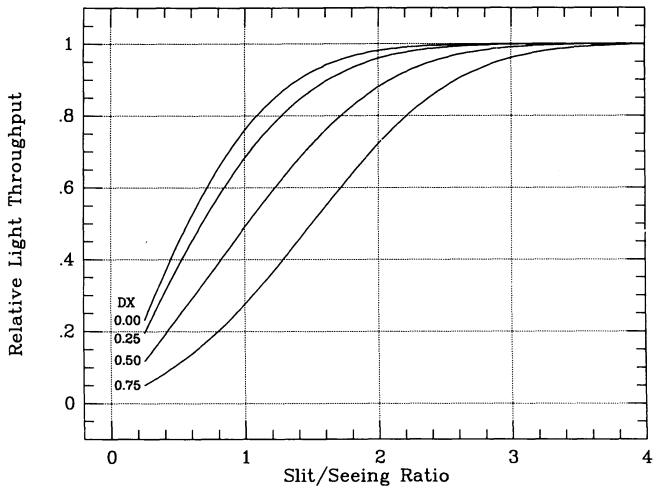

FIG. 1.—Plot of the fraction of light passing through a long slit as a function of the ratio of slit width to seeing size (FWHM) for four different centering errors: $DX = 0.00, 0.25, 0.50, 0.75$, where DX represents the miscentering in units of the seeing size. This diagram is taken from eq. (8) of Filippenko (1982) and assumes Gaussian stellar profiles. Note, however, that King (1971) has shown that a true stellar profile is more complex than a simple Gaussian.

to observe with a wide slit (4 arcsec) as well as a narrow slit (1.5 arcsec). For most spectrographs, especially those on large telescopes, opening the spectrograph slit to match the total angular size of the target leads to a serious degradation of the spectral resolution (e.g., under poor seeing conditions or for extended objects). Consequently, we observed using two settings: one wide setting which alleviates seeing effects (and the problems discussed in the next two paragraphs), and one narrow, or conventional, width setting. The wide setting provides wavelength-dependent correction factors that are applied to the line ratios derived from the narrow setting. The narrow setting is essential for measuring the weaker lines that are smoothed out by the poor spectral resolution of the wide setting.

Third, a measurement of the flux made through a narrow slit will underestimate the true flux due to seeing losses, improper positioning, and guiding errors if the standard stars were observed through a wide slit to avoid these problems. (Faint objects typically are observed through a narrow slit to improve the sky noise rejection and to maintain spectral resolution. On the other hand, a wide slit may be used for standard stars since these are bright and spectral resolution is unimportant.) If the standards are observed through a slit width similar to that used for the main observing program, then the measured program object flux can scatter to either higher or lower values than the true flux. In any case, proper photometric techniques (e.g., photomultipliers, CCD imaging) should be used if accurate ($\lesssim$2%) fluxes are required. Clearly, photometry is the preferred observational approach. However, approximate spectrophotometric fluxes ($\sim$15%) can be derived using the wide slit technique. Note that a wide slit width has a distinct advantage over a conventional slit width when estimating fluxes for MC PN, since these objects are often spatially extended (Jacoby 1980; Wood et al. 1987; Jacoby, Walker, & Ciardullo 1990).

Fourth, it is well known that the ionization structure changes across the face of most PNs. Because many of the MC PNs are extended, the spectrograph slit may fall on different positions in a given nebula from night to night or from observer to observer. This may be why some objects are reported

with different line ratios, despite being relatively bright and easy to observe.

A fifth problem arises when observing faint PNs in the MC. The background of the Clouds is littered with faint stars to such a degree that the definition of "sky" at any point along the slit becomes problematic. In addition, there may be no region along the slit where diffuse nebular emission is *not* present, thereby complicating matters even further. Figure 2 demonstrates a particularly bad case. The underlying stellar absorption systematically reduces the measured strength of the Balmer lines relative to the forbidden lines. At the same time the diffuse emission can affect any of the emission lines to an unpredictable degree. Long-slit spectroscopy provides a tool for estimating the magnitude of these effects, whereas fiber-optic or aperture spectroscopy (e.g., Boroson & Liebert 1989) can yield confusing measurements. These effects can introduce very large errors in the line strengths (e.g., factor of 2), and there is no general solution. At a minimum, long-slit spectroscopy provides the means to identify those cases where serious errors may be present, and it allows one to try improving the "sky" subtraction by choosing different "sky" positions along the slit after the observations are taken.

3. OBSERVATIONS

3.1. *Spectroscopy*

A short experimental observational run at Cerro Tololo (CTIO) on UT 1990 November 18 and 19 provided an opportunity to test the procedures described above to obtain improved spectrophotometry of faint MC PNs. The tests include a comparison of the line ratios and [O III] λ5007 fluxes between the CTIO results and those in the literature. Since the degree of discordance (if any) might be a function of apparent brightness, objects covering a wide luminosity range were observed.

The 4 m RC spectrograph was used with the Blue Air Schmidt camera and coated GEC CCD (385 columns by 576 rows). This configuration yields a spatial resolution along the slit of 0.73 arcsec per pixel. Grating 250 with a 1 mm GG 360 order separation filter was used for the "red" setting (λ3560–λ6810) on the first night to observe a total of 10 PNs in the SMC and LMC. Grating KPGL-2 was used for the blue spectral setting (λ3460–λ5120) on the second night to observe the 10 PNs from the previous night, plus two additional PNs. The wide slit observations were necessary only with the "red" setup since that instrumental configuration encompassed the entire spectral range of interest. The purpose of the blue setup was to provide superior spectral resolution in measuring important faint lines (e.g., λ4363), and to eliminate blending of interesting lines (e.g., $\lambda\lambda$4686, 4714, 4740). Seeing was typically $\sim$1.8 arcsec during the two night run; thus, wide slit measurement errors due to atmospheric effects should be smaller than 5% even with centering errors as large as 0.5 arcsec (see Fig. 1). The object list is given in Table 1, along with the exposure times.

Except for the 7.5 arcsec wide extraction aperture, data reduction followed common procedures for two dimensional

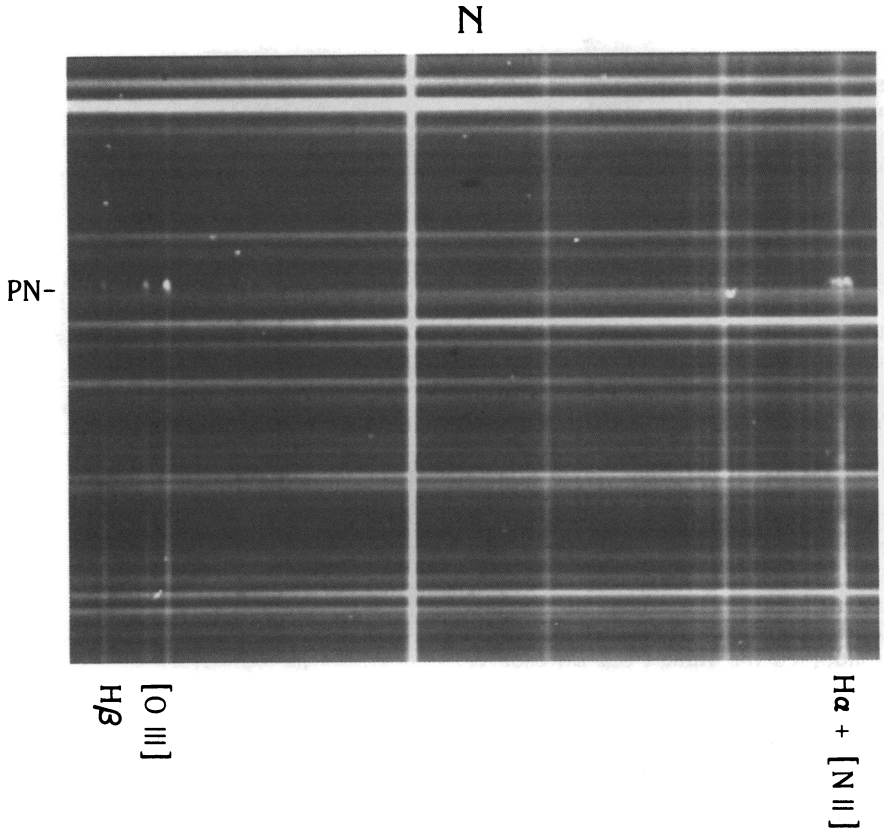

FIG. 2.—This magnified portion of the long-slit spectrum of LMC J22 is criss-crossed with numerous stellar spectra, diffuse emission lines, and night sky lines. A faint star, located $\sim$2.5 arcsec southwest of J22, complicates the process of extracting a one-dimensional spectrum of the PN from the two-dimensional image. Furthermore, the diffuse emission has different line ratios (e.g., Hβ/λ5007) than the PN, and so sky subtraction must somehow account for the underlying H II region contribution. It is almost impossible to identify a region along the slit where the H II region intensity is comparable to that near the PN and is also free of stellar continuum sources. These effects combine to introduce serious errors in the derived line ratios that approach a factor of 2, even for relatively strong lines such as Hβ.

TABLE 1

SPECTROSCOPY SUMMARY

PLANETARY	EXPOSURE (s)		
	Wide	Narrow	Blue
SMC 15	300	300	1200
SMC J6	1200	600	2700
SMC J18			1800
LMC 25	120	300	600
LMC 32	120	600	1200
LMC 54	100	600	1200
LMC 89	60	300	600
LMC 98	60	300	600
LMC 100			600
LMC J20	240	1200	2400
LMC J22	240	1800	1800
LMC J38	240	1200	1800

spectrophotometry. Standard IRAF version 2.9 packages were used throughout. Serious line blends such as the Hα + [N II] lines were deconvolved assuming Gaussian profiles. The wide slit data provided ratios for ~15 lines between λ3727 and λ6731 which were then used to correct the narrow slit flux ratios. However, only five and four lines, respectively, were measurable in the wide slit spectra of the very faint objects, LMC J22 and SMC J6. Consequently, the final line ratios for these objects are uncertain.

In general, the background (sky plus diffuse galaxy plus stars) was determined from an average of two sky "apertures," each measuring 15 arcsec in length, symmetrically about the object along the slit. For the more difficult cases, the sky position was chosen by visually examining the spectrum along the slit to find regions devoid of stellar continua and diffuse emission. In cases where the diffuse emission seemed to be "everywhere," line plots were made along strong emission lines (e.g., λ3727, λ5007, λ6563) to identify sky positions having intensities comparable to those adjacent to the PNs. Generally, this problem was not serious; determining the background level was especially troublesome, however, for LMC J20, J22, and J38, and the line ratios for these objects are very uncertain (see Fig. 2). Three representative examples of the spectra, ranging from best (*top*) to worst (*bottom*), are shown in Figure 3.

Line ratios corrected for extinction, Hβ fluxes derived from the wide-slit observations, both corrected, $I(\mathrm{H}\beta)$, and uncorrected for extinction, $F(\mathrm{H}\beta)$, and reddening constants, c, for the 12 objects are listed in Table 2. Values for c are calculated from the observed Balmer decrement (Hα/Hβ) and assuming a standard ratio of 2.85 (Brocklehurst 1971), except in the two instances where no red data are available (SMC J18 and LMC 100). For SMC J18, we adopted the value from Boroson & Liebert (1989): $c = 0.42$. For LMC 100, we adopted $c = 0$. We could use the observed ratios of Hγ/Hβ and Hδ/Hβ relative to standard values of 0.469 and 0.260. Note, however, that small observational errors can result in very significant uncertainties in c when doing so. For example, a 5% error in the ratio of Hγ/Hβ can cause an unreddened object to appear as if $c = 0.16$. In turn, this creates a 12% error in the corrected ratio of λ3727 relative to Hβ. Thus, line strengths are generally no better than ~10% for spectra that have been reddening-corrected using values for c derived solely from these ratios.

3.2. *Imaging*

Narrow-band images at λ5007 (full width at half-maximum of 28 Å) were obtained on UT 1991 December 6 and 8 for nine faint LMC PNs using the CTIO 4 m prime focus and a thinned Tektronix 1024 × 1024 CCD. In this f/2.7 configuration, the image scale is 0.477 arcsec per pixel. Seeing was typically 1.1 (objects J20, J22, J24, J35, and J38) and 1.8 (objects J4, J10, J21, and J26) arcsec on December 6 and 8, respectively. Exposure times were 300 seconds for all but J4, J10, and J21 which were observed for 600 seconds. Both nights appeared to be photometric based on standard star observations for which the measurements are consistent to ~1%. Atmospheric extinction during this period was likely to have been enhanced by the aerosols emitted from a variety of volcanos. We adopt 0.25 mag per air mass at λ5007 based on spectrophotometry made available by Jack Baldwin. This represents an increase of 0.08 mag per air mass over the usual λ5007 level.

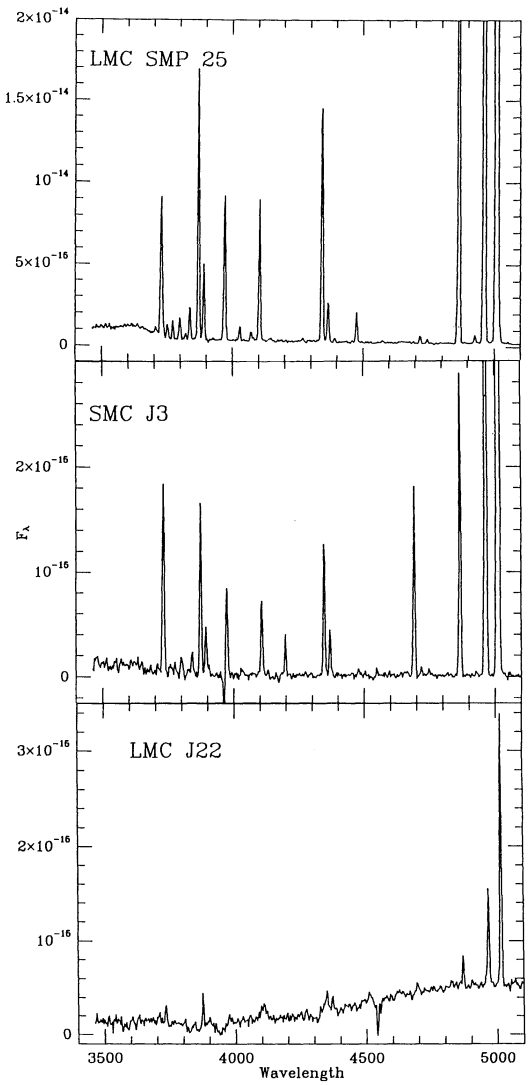

FIG. 3.—This spectral sequence extending from a bright PN (*top*) to a faint and difficult PN (*bottom*) is representative of the quality of the data. The spectra in the upper and middle panels have been stretched vertically to show the weaker lines. The continuum evident in the spectrum of LMC J22 illustrates that the stellar contamination shown in Fig. 2 was not removed completely during the spectral extraction.

TABLE 2

CORRECTED LINE RATIOS

λ	Identification	SMC 15[a,b,c]	SMC J6[d]	SMC J18[d]	LMC 25	LMC 32[b,e]	LMC 54[d,e]	LMC 89[a,b,f]	LMC 98[b,g]	LMC 100[g]	LMC J20[d]	LMC J22[d]	LMC J38[d]
3727	[O II]	14.4	81.4	32.5	34.3	76.1	315.4	42.5	45.1	28.8	459.1	73.9	398.0
3750	He II, H12	2.6	...	...	3.5	...	...	...	...	...	...	...	...
3770	H11, He II, O III	2.9	...	...	3.2	...	...	...	...	...	...	...	...
3798	H10	4.6	...	...	4.8	5.2	...	6.7	4.2	...	...	...	...
3835	H9	6.7	...	...	6.9	7.5	...	7.3	7.1	7.3	...	...	...
3868	[Ne III]	38.7	79.9	56.5	50.1	75.0	131.1	84.8	116.0	73.6	122.6	272.8	127.4
3889	H8, He I	11.8	...	...	14.6	16.0	...	14.8	16.7	15.8	...	...	21.2
3970	[Ne III], Hε	28.2	26.2	...	30.9	38.6	59.7	39.9	51.3	36.6	40.6	141.5	55.4
4026	He I	2.6	...	...	2.3	2.0	...	...	3.3	...	...	...	...
4067	[S II]	1.1	...	...	1.9	3.3	13.4	3.0	5.5	...	...	...	...
4077	[S II]	...	...	...	0.8	...	...	...	...	...	...	...	...
4101	Hδ	25.9	31.7	20.1	26.0	25.6	27.6	24.0	25.6	24.0	15.0	...	22.0
4267	C II	0.5	...	...	0.5	1.3	...	...	0.8	...	...	...	...
4340	Hγ	49.1	35.9	42.7	45.3	45.9	48.8	44.7	48.0	40.8	31.2	80.1	45.5
4363	[O III]	7.1	...	16.1	7.5	19.8	23.2	16.1	19.5	13.1	17.2	48.8	22.0
4388	He I	0.6	...	...	0.7	...	...	...	...	...	...	...	...
4471	He I	6.1	...	...	5.2	2.8	...	4.9	5.6	2.1	...	...	...
4686	He II	...	73.1	21.5	...	61.9	75.5	13.0	19.7	37.6	48.7	48.9	70.9
4714	[Ar IV], He I, [Ne IV]	1.4	...	...	1.3	4.6	6.5	2.7	3.1	4.0	...	...	...
4740	[Ar IV]	0.4	...	...	0.6	3.8	4.9	3.4	3.9	...	...	...	...
4861	Hβ	100.0	100.0	100.0	100.0	100.0	100.0	100.0	100.0	100.0	100.0	100.0	100.0
4921	He I	1.6	...	...	1.5	1.2	...	...	1.0	...	...	...	...
4959	[O III]	199.7	57.6	124.0	266.3	371.3	253.0	442.2	471.5	406.1	228.7	380.5	221.6
5007	[O III]	574.4	164.0	344.5	804.8	1094.6	761.7	1311.2	1417.0	1246.5	681.4	1041.0	651.0
5755	[N II]	0.6	...	...	0.8	...	15.1	1.1	...	...	15.8	22.1	16.0
5876	He I	18.2	...	...	16.3	8.5	9.9	15.8	14.4	...	10.5	...	11.8
6300	[O I]	2.9	16.9	...	4.4	8.7	34.3	9.8	9.1	...	25.0	...	31.3
6363	[O I]	0.09	...	...	0.9	1.8	9.0	3.0	3.3	...	...	...	6.8
6563	Hα	285.0	285.0	...	285.0	285.0	285.0	285.0	285.0	...	285.0	285.0	285.0
6583	[N II]	13.2	398.5	...	19.9	31.9	641.7	33.4	33.5	...	692.8	627.6	585.5
6678	He I	4.2	...	...	3.8	2.6	3.7	3.9	3.2	...	...	...	2.3
6717	[S II]	0.9	11.9	...	1.1	5.6	50.1	2.8	1.9	...	90.8	10.4	51.6
6731	[S II]	...	8.3	...	1.4	7.4	41.0	4.2	3.3	...	68.1	...	40.4
c		0.19	0.27	0.42	0.22	0.20	0.46	0.41	0.40	0.00	0.07	0.40	0.46
Log $F(\mathrm{H}\beta)$		−12.474	−14.482	−14.562	−12.384	−12.848	−13.418	−12.633	−12.578	−13.220	−13.878	−14.562	−13.693
Log $I(\mathrm{H}\beta)$		−12.28	−14.21	−14.14	−12.16	−12.65	−12.96	−12.22	−12.18	−13.22	−13.81	−14.16	−13.23

[a] For comparison, see Meatheringham & Dopita 1991a.
[b] For comparison, see Monk et al. 1988.
[c] For comparison, see Aller et al. 1981.
[d] For comparison, see Boroson & Liebert 1989.
[e] For comparison, see Meatheringham & Dopita 1991b.
[f] For comparison, see Aller 1983.
[g] For comparison, see Vassiliadis et al. 1992.

Instrumental magnitudes for the objects (including standards) were measured using an aperture having a diameter of 20 pixels (9.5 arcsec) and a concentric sky annulus having inner and outer diameters of 24 and 50 pixels (11.4 and 23.9 arcsec) respectively. Instrumental magnitudes were then converted to flux through observations of spectrophotometric standard stars following the prescription outlined by Jacoby, Quigley, & Africano (1987). Corrections for the effects of the converging beam of the telescope and ambient temperature changes on the transmission characteristics of the narrow-band filter were carried out according to Jacoby et al. (1989).

The determination of error estimates in the photometry is complicated by the fact that the objects vary from having stellar profiles to being moderately extended. For the former, the photometry should be very accurate ($\sim$2%) because a small measuring aperture ($\sim$4 arcsec) can be used to reduce the sky uncertainty (usually the dominant error source), in combination with an aperture size correction derived from 5–10 well exposed isolated stars on the same frame. The aperture correction is needed to provide consistency with the 9.5 arcsec aperture used for the standards. Photometry of extended objects may be affected by potential systematic errors since the 9.5 arcsec aperture used for those cases may include a slightly different fraction of the light for each object. We believe that this effect is small ($\lesssim$5%) since the object of largest extent (LMC J4) is still less than 4 arcsec in diameter. We estimate that the errors in these flux measurements are no worse than 5%.

The λ5007 fluxes for the nine PNs are given in Table 3. Unfortunately, we have only one object in common with the single other CCD imaging survey of MC PN. Jacoby et al. (1990, hereafter JWC) also observed LMC 54 (=J35) and the agreement between the two measurements is perfect. We measured the flux on December 6 and 8 to be 2.3% brighter and 1.5% fainter, respectively, than did JWC who estimated their uncertainty at 2%.

4. DISCUSSION

4.1. *Spectroscopy Comparisons*

Our spectrophotometry (Table 2) agrees extremely well with values in the literature, even for the fainter lines, as long as we restrict our attention to the brighter objects. In general, agreement for the bright objects is at the level of a few percent; discordance beyond 20%–30% is highly significant and yet there are a few outstanding cases where such extraordinary conflicts arise.

The most discrepant example is LMC 89 where we find that the blue lines, such as [O II] λ3727 and [Ne III] λ3868, are only $\sim$64% of that reported by Meatheringham & Dopita (1991a). Interestingly, Monk et al. (1987) also find weaker blue lines (e.g., 77%) for this object. On the other hand, Aller (1983) derives line strengths even weaker than ours, at 52% of the Meatheringham and Dopita levels. Thus, we have a situation where a reasonably bright nebula has been observed by four independent groups, the line strengths reported differ by as much as 50%, and for the specific instance of λ3727, no two groups agree to better than 15%! Part of the discrepancy with Meatheringham & Dopita (1991a) can be attributed to their larger value of the reddening parameter. This *may* be a consequence of the fact that they could not measure the reddening from the ratio of Hα to Hβ because Hα was a saturated line in their spectrum. Thus, they were forced to use the ratios of the weaker Balmer lines instead, a procedure that is sensitive to observational errors. An 8.5% error in the ratio of Hγ to Hβ is sufficient to account for the discrepancy in reddening values. However, a different reddening value can account for only one-third of the discrepancy in the blue line fluxes. A more subtle problem persists; perhaps this object is somewhat extended and exhibits unusually large ionization stratification, although we see no evidence in our long-slit spectrum for this speculation. An even less likely conjecture is that the nebula is variable.

When we consider the fainter objects from the Jacoby (1980) sample, we expect the agreement to be somewhat less satisfying, partly due to poorer photon statistics, but also because of the potential problems discussed in § 2, plus the fact that these objects are generally invisible on acquisition TV systems. This last obstacle could lead to gross pointing errors with a consequent tendency toward systematic trends in the spectrum as a function of wavelength that depend on the observational tactics of the different investigators. However, it is evident in some cases that background subtraction errors dominate the comparison. This is demonstrated dramatically by the factor of 2.5 difference with respect to Boroson & Liebert (1989) for the λ4340 line in LMC J22. Normally, one expects to be able to measure this relatively bright line to an accuracy of 10%–20%. There are also some remarkable differences such as λ3727 in SMC J6 and SMC J18 which exhibit a factor of 2 discrepancy, and the extreme factor of 4 difference at λ3868 for SMC J18.

Our wide slit data for the very faint SMC J6 is virtually useless; the low flux from the object, combined with the degraded spectral resolution, nullifies any benefit gained in circumventing the atmospheric problems with the wide slit. Also, we did not obtain a "red" setting for SMC J18 and so we do not have wide slit data, nor do we have a good measurement of the reddening for this object. However, the large differences we see in these instances cannot be attributed to a lack of wide slit data. It is more likely due to background subtraction errors. A much more imaginative explanation for SMC J18, at least, is that Boroson & Liebert (1989) observed a different faint PN than we did! The coordinates given by Jacoby (1980) indicate the PN is to the east of the coordinate reference star, but his finding chart shows the PN to be to the west. It is the latter object which we observed.

We conclude that the spectral data reported in the literature for the bright objects generally are extremely reliable. Results for the faint objects are less reliable. As typified by the deviations for the intermediate brightness object LMC 54 (=J35), ratios for the brighter lines in the fainter objects should be accurate to $\sim$25%.

TABLE 3

λ5007 FLUXES AND DIAMETERS

Planetary	Log $F_{\lambda 5007}$	Diameter
LMC 54	−12.460	1″.32
LMC J4	−13.350	3.86
LMC J10	−13.426	2.62
LMC J20	−12.928	1.82
LMC J21	−13.205	2.10
LMC J22	−13.372	0.00
LMC J24	−13.388	0.55
LMC J26	−12.904	2.73
LMC J38	−12.748	1.34

4.2. *Photometry Comparisons*

We first compare the λ5007 CCD fluxes for the nine PNs with the photographic results given by Jacoby (1980). To improve the statistics of the comparison, we also include data for the eight brighter PNs in the Jacoby (1980) catalog that were observed by JWC. Figure 4 illustrates that the photographic data are consistent with Jacoby's error estimate of 0.25 mag. The principal exceptions are the three "bracket" magnitudes, which are really fluxes measured from red plates, corrected for an assumed contribution from the [N II] lines, and then assigned [O III] fluxes based on an assumed ratio of λ5007 to Hα. Clearly, the "bracket" fluxes are unreliable. Rejecting those objects yields a mean error of 0.33 mag with a zero-point offset of 0.12 mag in the sense that the photographic data are too faint. If we also reject the single photographic entry (LMC J21) for which the calibration curve required extrapolation (Jacoby 1980), then the average error is reduced to 0.26 mag and the zero-point error is reduced to 0.06 mag. In general, the Jacoby (1980) fluxes appear to be useful, although the "bracket" magnitudes are not, and magnitudes requiring extrapolation of the calibration curves should be considered questionable.

Figure 5 shows that the agreement is poor between the CCD photometry and the spectrophotometric fluxes given by Boroson & Liebert (1989). Those authors discuss some of the reasons for potential differences between their fluxes and those given by Jacoby (1980). Their worst case example, LMC J26, is 2.84 mags fainter than Jacoby's (1980) value. Our CCD imaging flux, however, is in fair agreement with Jacoby, being fainter by only 0.18 mag. Discrepancies of several magnitudes are difficult to understand, leading us to conclude that the Boroson & Liebert (1989) fluxes should not be used, especially for the faint PNs.

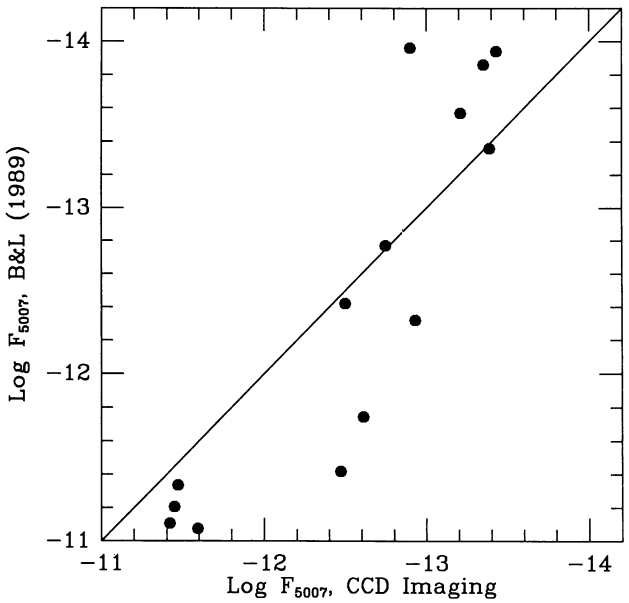

FIG. 5.—λ5007 fluxes reported by Boroson & Liebert (1989) are compared to the CCD imaging data. Serious discrepancies are evident.

We next compare our spectrophotometric fluxes with our CCD photometry and the CCD photometry of the brighter PNs by JWC. Figure 6 shows that a very good correlation exists; the dispersion is only 12%. (We ignore the value for

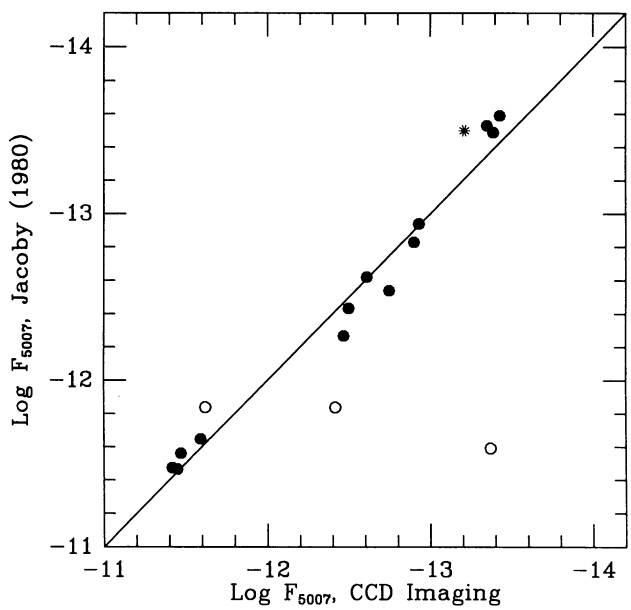

FIG. 4.—λ5007 fluxes measured photographically by Jacoby (1980) are compared to the CCD imaging results. The open circles are those PNs for which Jacoby converted red magnitudes to λ5007; obviously, these are subject to large errors. The asterisk(*) represents LMC J21 which required an extrapolation of the photographic calibration curve. Overall, the agreement with the CCD data is good, having a dispersion of 0.26 mag and an offset of 0.06 mag after rejecting the red magnitudes (*open circles*) and LMC J21. It may be that the photographic data exhibit a slightly nonlinear transformation such that bright and faint objects are measured too faint while the intermediate brightness objects are measured too bright.

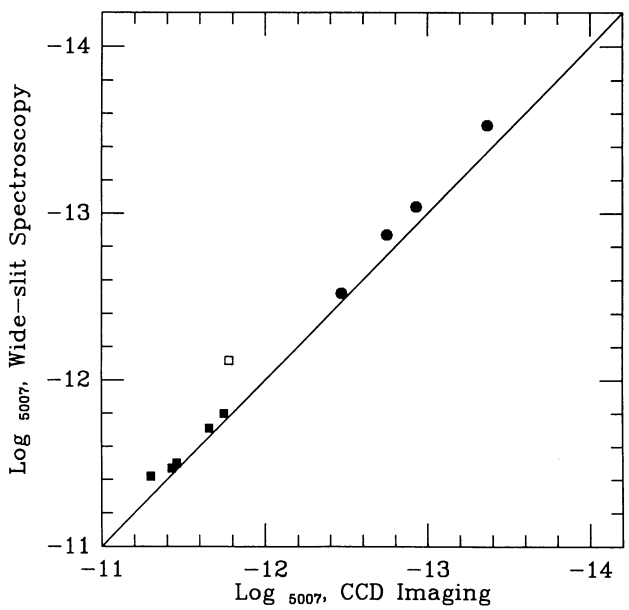

FIG. 6.—λ5007 fluxes measured from the wide-slit data are compared to the CCD imaging data. Squares represent CCD data obtained by Jacoby et al. (1990); LMC 100 is shown as an open square since it was observed only with a narrow-slit and consequently was measured too faint. The agreement with the CCD imaging data is very good, having a dispersion of 0.12 mag and an offset of 0.20 mag (spectra report the fluxes as being too faint). This offset, however, is much larger than expected (see Fig. 1) from the seeing conditions (<2 arcsec) while using a 4 arcsec slit. This may be due to improper telescope focus or systematically worse than expected centering. Nevertheless, with the photometric offset calibrated, the measurement precision is acceptable.

LMC 100 since we didn't observe this PN with a wide slit. The narrow-slit flux value is shown in the figure for completeness.) There is a zero-point shift, however, such that the spectral fluxes are all too faint by an average of 0.20 mag. In addition, there is a suggestion that the spectrophotometric fluxes for the fainter PNs are being measured increasingly too faint. This effect might arise if the fainter PNs are also the more evolved, and hence, more spatially extended, so that the 4 arcsec wide slit is systematically too small for faint objects. Alternatively, this effect could be due to inaccurate sky subtraction procedures or poor centering of very faint objects in the slit. Generally, the wide-slit spectrophotometric results appear to be reliable, provided the 0.20 mag zero-point correction is applied. We have applied this correction (0.08 dex) to the Hβ fluxes given in Table 2.

4.3. *Diameters*

The CCD images demonstrate that many of the MC PNs can be spatially resolved quite easily. Considering that the seeing was never better than 1 arcsec, these data indicate that accurate diameters, and possibly even morphological studies, may be possible with some of the newer technology telescopes, detectors, and computer processing techniques that routinely produce subarcsecond images.

Diameters of the nine PNs are included in Table 3. These were calculated following Wood et al. (1987) and Jacoby (1980) by subtracting the FWHM of stars in the frame from the PN FWHM in quadrature. JWC followed this course as well but they derived diameters smaller than those reported by Wood et al. (1987). Our results are mixed; our diameter of 1.3 arcsec for LMC 54 (=J35) is larger than the diameter of 0.9 arcsec given by JWC, our diameters for LMC J4, and J20 are in excellent agreement with the Wood et al. results, but our values for J10 and J26 (2.6 and 2.7 arcsec) disagree with the Wood et al. results of less than 1.1 and 3.2 arcsec, respectively. We suspect that the simple quadrature deconvolution is not very robust since it is measuring small deviations that are quite sensitive to morphological variations and atmospheric effects. For example, LMC J20 is clearly extended more in one direction than the other, and is reminiscent of a large bipolar such as NGC 650−1 (see Fig. 7 [Pl. 19]). The FWHM is not really meaningful in this case.

Images of the three most interesting objects are reproduced in Figure 7. LMC J20 was mentioned above; LMC J4 is the largest object in this study and is nearly resolved to the point of discerning a ring structure; LMC 54 (=J35) exhibits a very low surface brightness north-south emission structure having an extent of nearly 7 arcsec (1.7 pc).

Jacoby (1980) estimated the diameter of LMC J30 at 1.16 arcsec. Boroson & Liebert (1989) flagged this object as a false identification, concluding that it is not a PN, but rather a late-type star. Our CCD image of LMC J26 includes the field of J30, but a search at that position failed to identify any object whatsoever. Apparently, LMC J30 was a plate flaw and should be dropped from Jacoby's catalog.

4.4. *Compositions and Stellar Masses*

The compositions of these nebulae are given in Table 4, where we use the methods described in Kaler & Jacoby (1990). Helium compositions are given relative to hydrogen; oxygen compositions are given relative to 20^{-4} that of hydrogen. We used the code ABUNDR (Kaler 1985), which computes electron temperatures from [O III] and [N II], densities from [S II], [O II], and other p^3 doublets, and ionic abundances, all from standard procedures and the most recent atomic parameters. Elemental abundances are computed by summing ionic abundances and by using standard ionization correction factors for the missing ions: $(O^{3+} + O^{4+})/(O^+ + O^{2+}) = He^{2+}/He^+$ and $N/O = N^+/O^+$. C/O ratios are derived from λ4267 and Kaler's (1983) algorithm. In cases where the auroral lines of [O III] or [N II] were not observed, we estimated the [O III] and [N II] electron temperatures according to the strength of the He II λ4686 line and Kaler's (1986) correlations. In the instances in which [S II] was absent, we used [O II] from the literature or estimated the density on the basis of the stellar luminosity (which correlates with nebular diameter) and the correlations given by Kaler & Jacoby (1990). No density is known for LMC 100, so 1000 cm^{-3} was assumed, which makes the abundances rather uncertain. For SMC J18 we borrowed red data (from which we also derive the interstellar extinction constant) from Boroson & Liebert (1989).

Central star temperatures and luminosities (T_* and $L_*/L_\odot$) are given in Table 5. For high-excitation nebulae, those with He II lines, they were derived by the crossover method devel-

TABLE 4

CHEMICAL COMPOSITIONS

Nebula	T[O III][a]	T[N II][a]	N_e[b]	O^+	O^{++}	O/H	He^+	He^{++}	He/H	N/O	C/O	Comments
SMC 15	12100	14100	8700	0.04	1.23	1.27	0.110	...	0.110	0.39	1.13	c
SMC J6	16700*	12400*	(200)	0.11	0.16	...	...	0.069	...	3.5	...	
SMC J18	26800	12400*	(200)	0.03	0.14	...	...	0.021	...	18	...	d
LMC 25	11400	15700	1800	0.04	2.00	2.04	0.105	...	0.105	0.45	0.54	e
LMC 32	14700	11300*	1700	0.02	1.44	3.15	0.060	0.057	0.117	0.21	1.29	e
LMC 54	18600	11800	200	0.43	0.59	1.80	0.094	0.072	0.166	1.35	...	
LMC 89	12900	13500	3000	0.074	2.35	2.71	0.098	0.011	0.109	0.48	...	e
LMC 98	12800	11300*	4640	0.016	2.56	3.24	0.092	0.017	0.109	0.29	...	e
LMC 100	12500	11300*	1000	0.09	2.38	4.28	0.047	0.034	0.081	...	...	e, f
LMC J20	21700	11700	300	0.06	0.38	1.48	0.081	0.046	0.128	0.95	...	
LMC J22	17700	14600	(100)	0.06	0.90	...	...	0.046	...	7.6	...	
LMC J38	20600	12700	200	0.39	0.41	1.44	0.085	0.068	0.153	1.09	...	

[a] Asterisks(*) on T_e mean value found from He II and Kaler 1986.
[b] Parentheses around N_e mean value derived from L_*. All other N_e are from [S II] except for SMC 15 (see note c).
[c] Uses mean [O II] density from Dopita et al. 1988 and Barlow 1987.
[d] Red data from Boroson & Liebert 1989.
[e] New object.
[f] No density available, 1000 cm^{-3} adopted.

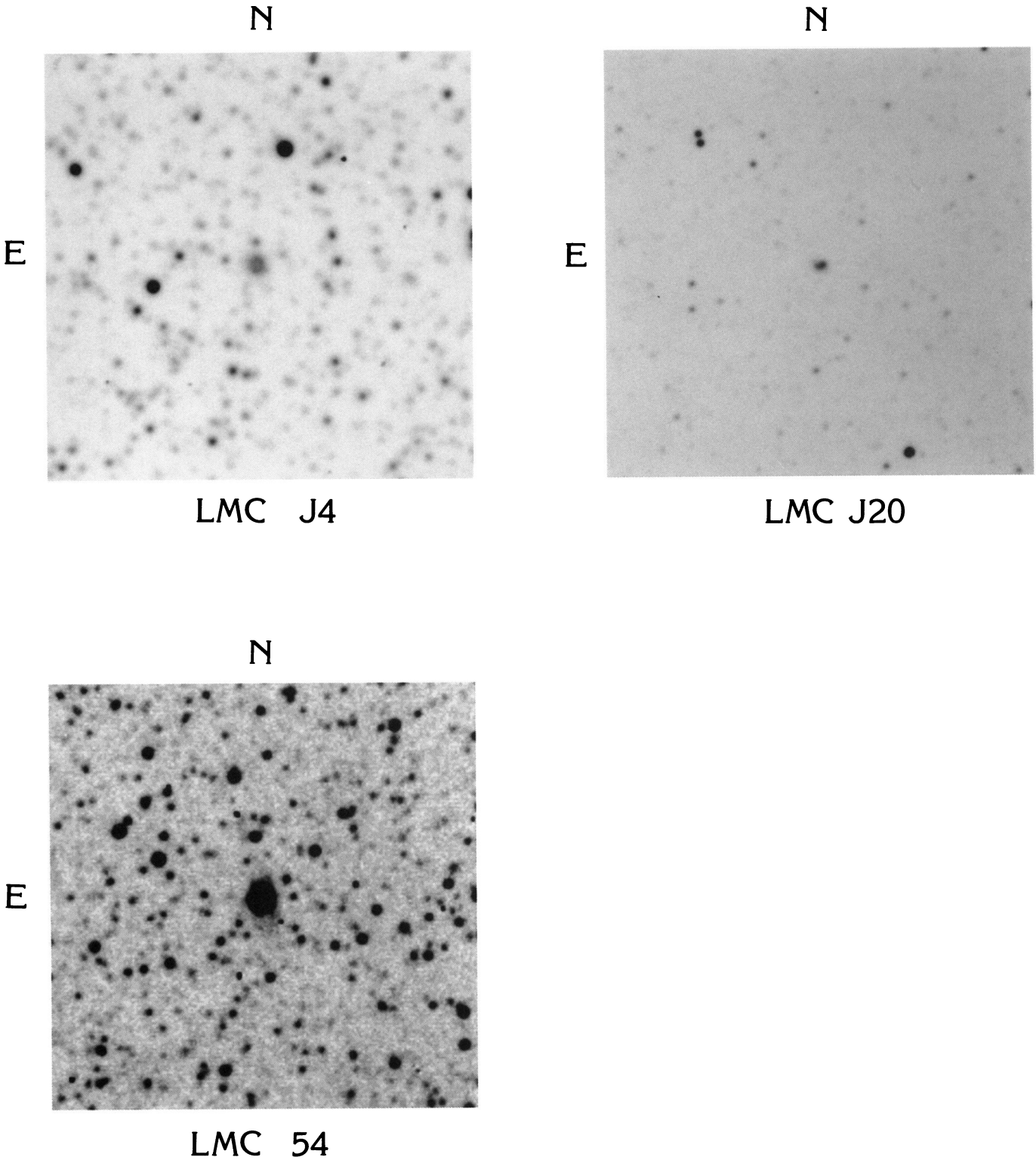

FIG. 7.—Images of the three most morphologically interesting PNs. North is up and east is to the left; each image is 90 arcsec on a side. LMC J4 has a diameter of 3.86 arcsec and displays a distinct disk, possibly with a central diminution of light suggestive of a ring or shell. LMC J20 shows a clear bilobed structure having an extent of ~2 arcsec. LMC 54 is surrounded by a very extended, low surface brightness, structure running along the north–south direction for 7 arcsec (1.7 pc).

JACOBY & KALER (see 417, 216)

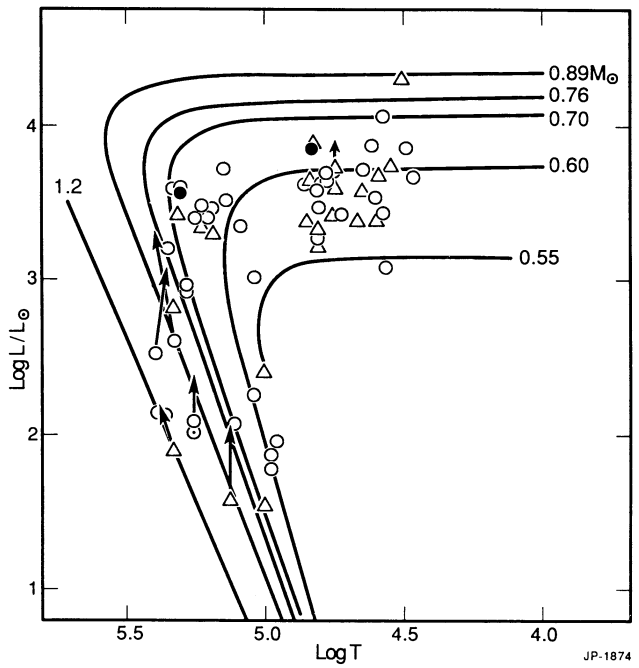

FIG. 8.—log L–log T plane from Kaler & Jacoby (1991), in which circles and triangles, respectively, represent objects in the LMC and the SMC. New points are plotted directly as filled symbols. Changes from old values are represented by the tips of the arrows. The dot inside one point shows that it did not significantly change its position.

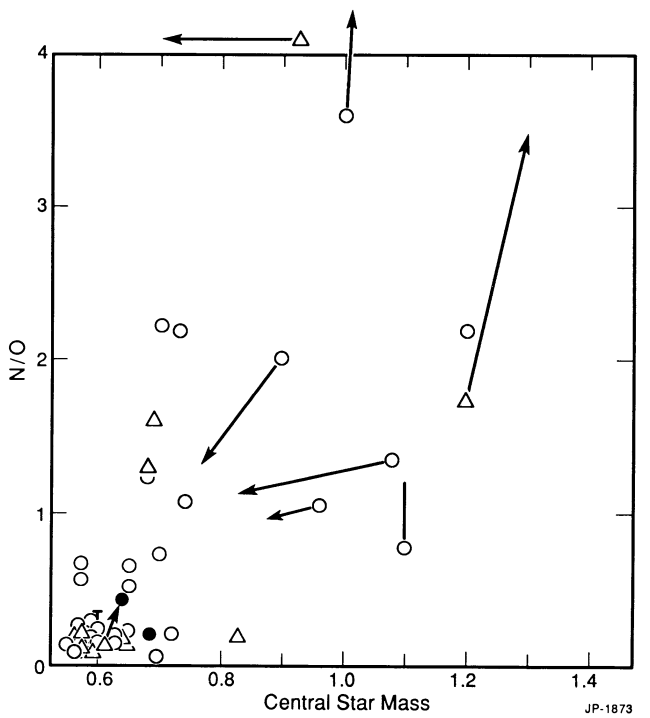

FIG. 9.—N/O vs. M_c for the full set of objects from Kaler & Jacoby (1990, 1991) as per the symbolism of Fig. 8. The vertical bar with no arrowhead represents a possible range in N/O.

oped by Kaler & Jacoby (1989, 1900), in which we find the central star magnitude that equates the H and He II Zanstra temperatures for nebulae considered optically thick on the basis of strong [O II]. Only LMC 89, 98, and 100 did not qualify, and so stellar parameters are not given for these three nebulae. The two low-excitation nebulae (those for which He II is absent), SMC 15 and LMC 25, were assumed to be optically thick; however, without a λ4686 measurement a different scheme had to be used to derive T_* and $L_*/L_\odot$. We adopted the method outlined by Kaler & Jacoby (1991) which approximates the Stoy temperature from the strength of λ5007.

We then placed the stars on the log L–log T plane along with the standard evolutionary tracks used by Kaler & Jacoby (1991) (Fig. 8) to determine stellar masses ($M_*/M_\odot$), which are also given in Table 5. To show how observational uncertainties translate here into astrophysical quantities, we show all old data and indicate the changes by arrows in the subsequent figures. The old data used by Kaler & Jacoby (1990, 1991) are based primarily on the compilations by Monk et al. (1988), Boroson & Liebert (1989), Meatheringham & Dopita (1991a), and Aller et al. (1981).

We next plot N/O, He/H, and C/O against central star mass in the same way in Figures 9 through 12. Figures 9 and 10, respectively, show N/O for the whole set of objects from Kaler & Jacoby (1990, 1991) and detail for N/O < 0.9. The new data reveal how sensitive the results can be to observational errors, but still support the correlation; if anything, it is strengthened. The new results clearly strengthen the helium correlation (Fig. 11). However, it is disconcerting that all five changes show

TABLE 5

STELLAR PARAMETERS

Nebula[a]	T_* (K)	$L_*/L_\odot$	$M_*/M_\odot$
SMC 15	54,000	7350	0.63
SMC J6	235,000	150	1.2
SMC J18	127,000	115	0.71
LMC 25[b]	65,000	6890	0.63
LMC 32[b]	207,000	3780	0.68
LMC 54	242,000	2110	0.77
LMC J20	179,000	235	0.87
LMC J22	180,000	105	1.0
LMC J38	229,000	1080	0.83

[a] LMC 89, 98, and 100 do not meet criteria for high optical depth, so stellar parameters cannot be found.
[b] New Object.

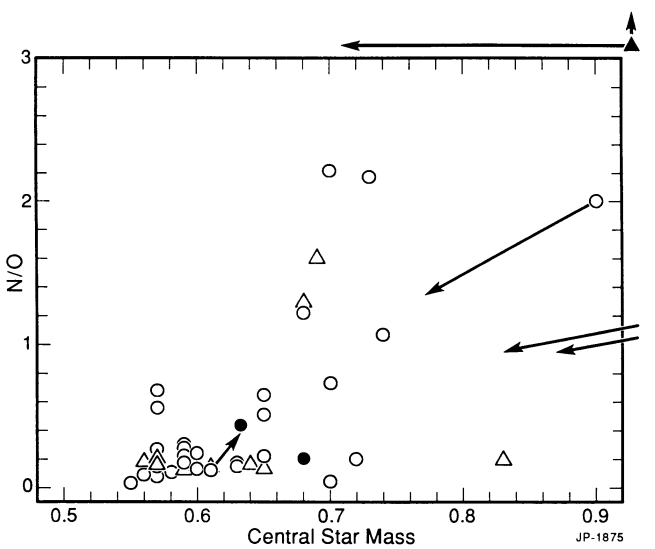

FIG. 10.—Fig. 9 expanded to show the detail in the N/O vs. M_c relation for lower mass as per the symbolism of Fig. 8.

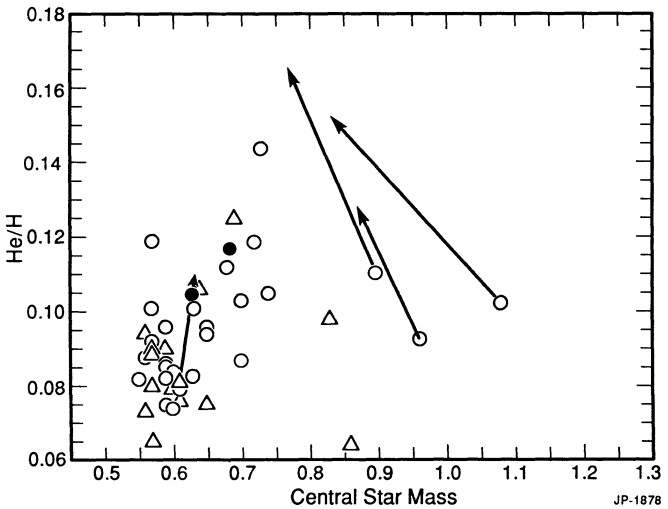

FIG. 11.—He/H vs. M_c from Kaler & Jacoby (1991) with new objects and changes made as per the symbolism of Fig. 8.

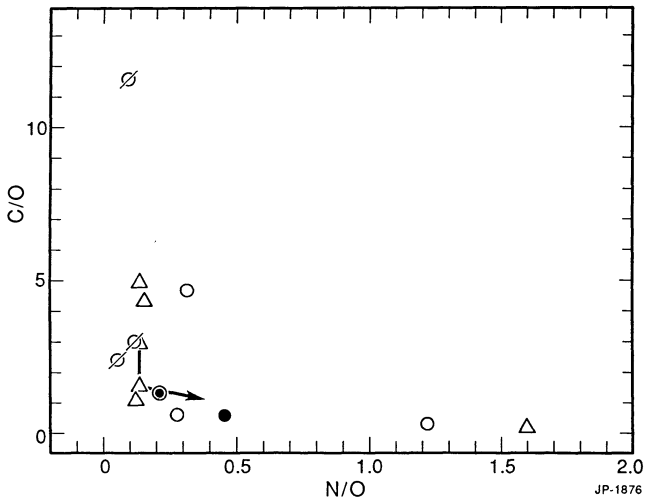

FIG. 13.—C/O vs. N/O from Kaler & Jacoby (1991) with objects and changes made as per the symbolism of Fig. 8.

increases in He/H, especially when in Kaler & Jacoby (1991) we chose to adopt the lower He/H values of Monk et al. (1988) instead of the slightly higher ones of Dopita & Meatheringham (1991). In support of the He/H ratios, there are no significant systematic differences between the He I ratios individually derived from λ4471, λ5876, and λ6678. Nevertheless, the changes show the difficulty of evaluating abundances from faint lines that are competing against stellar continua from crowded backgrounds (Fig. 2).

The three new carbon points in Figure 12 may still be consistent with the suggestion that C/O first increases with core mass, comes to a maximum, then decreases (Kaler & Jacoby 1991), although the data remain sparse. C/O apparently does anticorrelate strongly with C/N (Walton et al. 1991) and N/O (Kaler & Jacoby 1991). Unfortunately, there are no new extreme carbon or nitrogen values among the objects for which we observed λ4267, so the new points and the correction in the C/O versus N/O plot in Figure 13 do not extend the anticorrelation.

Finally, we apply the new data to the tentative correlation we posed in Kaler & Jacoby (1991) between O/H and central star mass. As before, we place the O/H from the two Clouds on the same scale by multiplying those of the Small Cloud by 2.2. In Figure 14 we shift two points into an area that was earlier seen to be relatively blank. However, we add new high-mass points (plus one from Kaler & Jacoby 1990), and with one exception, they all have lower O/H ratios; that is, there seems to be a decline in the upper limit of O/H as central star mass increases. Theory does not predict any such correlation, and further observations are needed to confirm or reject it.

This work was supported in part by National Science Foundation grants AST 88-13686 and AST 91-15030 to the University of Illinois. We would like to thank Louise Browning for her help with the figures, Robin Ciardullo for his help with the tables, and Mike Dopita for a careful reading of the manuscript and suggestions for its improvement. Also, we are grateful to Alex Filippenko for discussions clarifying aspects of his 1982 paper.

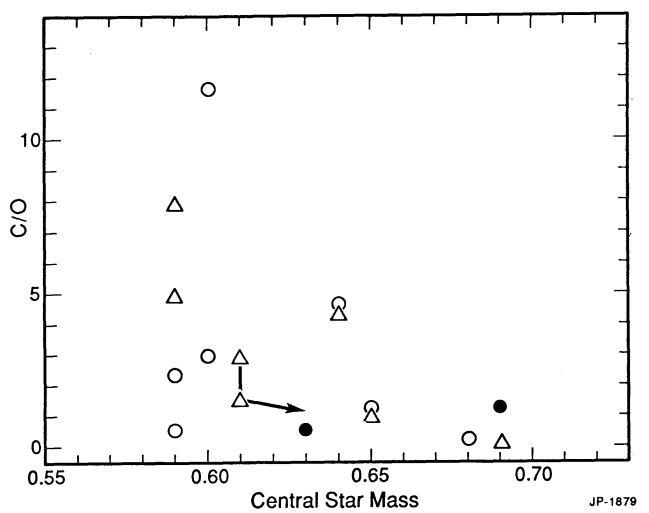

FIG. 12.—C/O vs. M_c from Kaler & Jacoby (1991) with new objects and changes made as per the symbolism of Fig. 8.

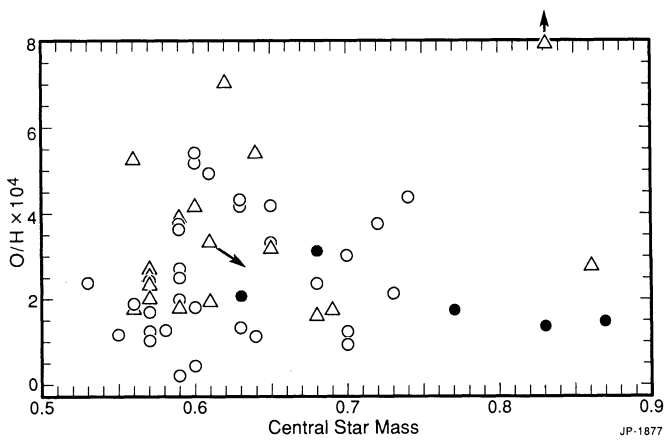

FIG. 14.—O/H vs. M_c from Kaler & Jacoby (1991) with new objects and changes made as per the symbolism of Fig. 8.

REFERENCES

Aller, L. H. 1983, ApJ, 273, 590
Aller, L. H., Keyes, C. D., Maran, S. P., Gull, T. R., Michalitsianos, A. G., & Stecher, T. P. 1987, ApJ, 320, 159
Aller, L. H., Keyes, C. D., Ross, J. E., & O'Mara, B. J. 1981, MNRAS, 194, 613
Barlow, M. J. 1987, MNRAS, 227, 161
Boroson, T. A., & Liebert, J. 1989, ApJ, 339, 844
Boyd, R. W. 1978, J. Opt. Soc. Am., 68, 877
Brocklehurst, M. 1971, MNRAS, 153, 471
Dopita, M. A., & Meatheringham, S. J. 1991, ApJ, 377, 480
Dopita, M. A., Meatheringham, S. J., Webster, B. L., & Ford, H. C. 1988, ApJ, 327, 639
Filippenko, A. V. 1982, PASP, 94, 715
Fried, D. L. 1966, J. Opt. Soc. Am., 56, 1372
Jacoby, G. H. 1980, ApJS, 42, 1
Jacoby, G. H., Ciardullo, R., Ford, H. C., & Booth, J. 1989, ApJ, 344, 704
Jacoby, G. H. Quigley, R. J., & Africano, J. L. 1987, PASP, 99, 672
Jacoby, G. H., Walker, A. R., & Ciardullo, R. 1990, ApJ, 365, 471 (JWC)
Kaler, J. B. 1983, IAU Symp. 103, Planetary Nebulae, ed. D. R. Flower (Dordrecht: Reidel), 245
———. 1985, ApJ, 290, 531
———. 1986, ApJ, 308, 322
Kaler, J. B., & Jacoby, G. H. 1989, ApJ, 345, 871
———. 1990, ApJ, 362, 491
———. 1991, ApJ, 382, 134
Meatheringham, S. J., & Dopita, M. 1991a, ApJS, 75, 407
———. 1991b, ApJS, 76, 1085
Monk, D. J., Barlow, M. J., & Clegg, R. E. S 1988, MNRAS, 234, 583
Sanduleak, N., MacConnell, D. J., & Philip, A. G. D. 1978, PASP, 90, 621
Vassiliadis, E., Dopita, M. A., & Morgan, D. H. 1992, preprint
Walton, N. A., Barlow, M. J., Monk, D. J., & Clegg, R. E. S. 1991, in IAU Symp. 148, The Magellanic Clouds, ed. R. Haynes & D. Milne (Dordrecht: Kluwer), 334
Wood, P. R., Meatheringham, S. J., Dopita, M. A., & Morgan, D. H. 1987, ApJ, 320, 178